Energy Conversion and Management 340 (2025) 119989

Contents lists available at ScienceDirect

Energy Conversion and Management

journal homepage: www.elsevier.com/locate/enconman

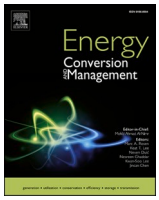

Exploration of co-gasification mechanism of sewage sludge and bituminous coal based on reactive force field molecular dynamics simulation

Jian Gao [a], Weiwei Xuan [a,b,*], Erzhou Zhang [a], Yaqiong Wang [b], Jiansheng Zhang [b,c], Qi Wang [d]

[a] School of Energy and Environmental Engineering, University of Science and Technology Beijing, Beijing 100083, China
[b] Shanxi Research Institute of Huairou Laboratory, Shanxi, Taiyuan 030032, China
[c] Department of Thermal Engineering, Tsinghua University, Beijing 100084, China
[d] Department of Inorganic Nonmetallic Materials, School of Materials Science and Engineering, University of Science and Technology Beijing, Beijing 100083, China

ARTICLE INFO

Keywords:
Sewage sludge
Bituminous coal
Co-gasification
ReaxFF-MD

ABSTRACT

The co-gasification of sewage sludge and coal not only facilitates industrial decarbonization but also provides a promising approach for sludge treatment. In this study, the mechanisms of sewage sludge and bituminous coal were explored by the molecular dynamic simulation and the reactive force field. Synergy analysis revealed that the co-gasification process enhanced the production of H_2 and CO by 2.1 % and 1.75 % respectively. The visualization results demonstrate that glyceryl triacetate, leucine, β-D-glucose and coal molecules decompose sequentially to produce fragments during the pyrolysis stage. In the initial gasification stage, a large number of OH radicals participate in the reactions, attacking the fragments into small-molecule highly reactive groups. While H radical is more readily react with the small reactive groups to generate gaseous products. Additionally, molecular cleavage is induced by high temperature and the interaction between OH radicals and molecular fragments is accelerated. More OH and H radicals are generated by using steam, further modulating the H_2/CO ratio. This study offers valuable molecular insights for optimizing the co-gasification process of sludge and coal and decarbonization goals.

1. Introduction

The continuous use of fossil fuels has led to the accumulation of carbon emissions, thereby causing severe global climate change and environmental degradation [1]. In response to these critical realities, major countries such as the United States, the European Union, and Japan have committed to achieving carbon neutrality by 2050 [2]. China has also demonstrated its consistent commitment to peaking CO_2 emissions before 2030 and achieving carbon neutrality by 2060 [3]. As the cornerstone of traditional energy, coal's reserve depletion is destabilizing energy supply systems [4], thereby developing the development of sustainable alternative energy sources a top priority. Focusing on the energy consumption structure, the industrial sector is one of the largest energy consumers. By 2021, it accounted for more than one-third of the global total final energy consumption, and 45 % of direct carbon dioxide emissions [5]. Therefore, industrial decarbonization is a significant challenge for these nations and a critical factor in achieving their carbon neutrality goals [6].

An effective industrial decarbonization strategy must consider the positive economic, social, and environmental impacts across a range of regions, including urban and industrial zones [7]. The sewage sludge (SS) generated from urban and industrial wastewater treatment has become a severe pollution issue [8]. In China alone, annual SS emissions approach 40 million tons [9]. SS consists of a large amount of organic substances, rich in various heavy metals and pathogens [10]. This complexity threatens ecological balance and health, while adding to the challenges of carbon management [11]. Traditional disposal methods such as landfills accelerate ecosystem pollution and miss opportunities for carbon recovery [12]. In recent years, thermochemical conversion technology has been widely applied in the field of sludge disposal. The inherent characteristics of SS, including low calorific value and high water content, restrict its combustion and pyrolysis processes [13]. In contrast, SS gasification efficiently converts sludge into gas fuel [14]. Therefore, co-gasification of SS and coal is a promising treatment method. It can partially substitute fossil fuels, which is of great significance for industrial decarbonization efforts [15].

* Corresponding author.
E-mail address: xww@ustb.edu.cn (W. Xuan).

https://doi.org/10.1016/j.enconman.2025.119989
Received 23 February 2025; Received in revised form 19 May 2025; Accepted 21 May 2025
Available online 27 May 2025

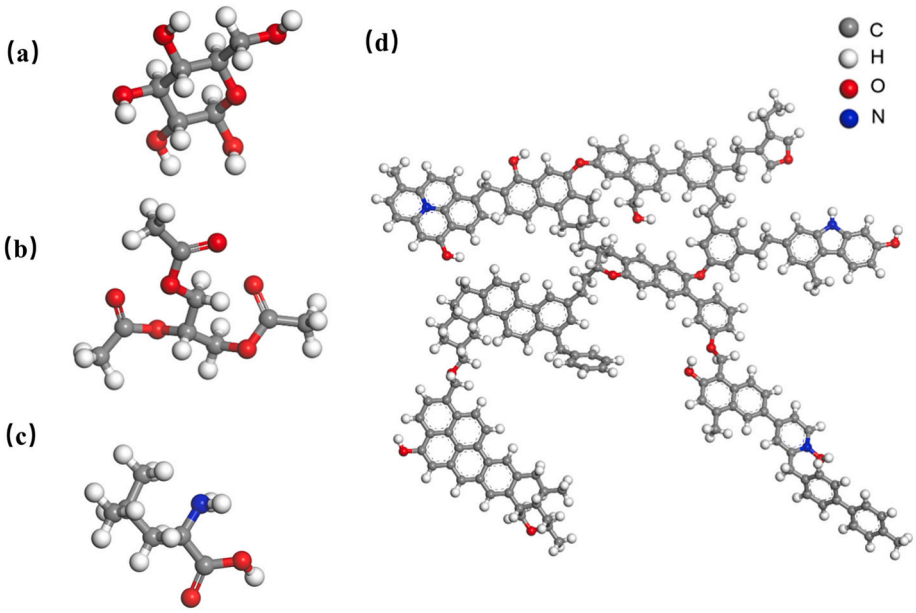

Fig. 1. Molecular structure of components (a) monomeric β-D-glucose molecule; (b) glyceryl triacetate molecule; (c) leucine molecule; (d) bituminous coal molecule.

Most of the existing research on the co-gasification of SS and coal mainly focuses on the optimization of product distribution and process parameters. Researchers have investigated the co-gasification of SS with lignite [16], bituminous coal [17], and anthracite [18], exploring various influential factors such as blending ratios, temperature, and pressure. The results have demonstrated that the synergistic effects in co-gasification are highly significant. Thus, many researchers have employed traditional experimental approaches to elucidate the mechanisms. For example, through GC–MS and high-performance liquid chromatography (HPLC) detection experiments, Wang et al. [19] found that phenol disrupts the conjugated structure by interacting with polycyclic aromatic hydrocarbons, thereby inhibiting coke formation. Ma et al. [20] used GC–MS experiments to detect liquid products and combined FTIR experiments to analyze the functional groups of solid products. Their research demonstrated that the demethylation and dehydroxylation of intermediate products boost the gasification performance, and also made known the transfer mechanism of three-phase product during the co-gasification. However, traditional experimental methods are limited by spatiotemporal resolution and it is difficult to track the bond-breaking and radical evolution processes in real-time [21,22]. This limitation hinders the investigation of decarbonization potential in co-gasification processes.

In recent years, molecular dynamics (MD) simulation technology has been widely used in fields such as materials science and chemical engineering. For instance, Zhou et al. [23] revealed the performance of a Ni-coated MoS2 membrane, elucidating its catalytic mechanism and separating process by using MD simulation. Adela et al. [24] observed the semi-solid stratification mechanism of $NaNO_3$ molten salt doped with SiO_2 nanoparticles through MD simulation and explained the reasons for the unconventional C_p increment. Xia et al. [25] clarified the absorption process of Aspergillus oryzae lipase (AOL) on the surface of ZIF-8 through MD simulation. Notably, ReaxFF-MD simulations demonstrate unique advantages in the field of thermal conversion, enabling the precise capture of reaction kinetic characteristics at the atomic scale [26,27]. Taking previous research work as an example [28], the ReaxFF-MD method was employed to perform in-depth analysis during the exploration of lignite and PE co-pyrolysis. This approach successfully revealed the synergistic mechanism among free radicals and offered insights for the efficient utilization of coal resources. Wang et al. [29] also achieved remarkable research results in the ReaxFF-MD simulation study of cationic resin SCWG. They elaborately disclosed the detailed decomposition process of cationic resin in supercritical water (SCW). Yu et al. [30] elucidated the N transformation pathways during coal/NH3 co-pyrolysis by using ReaxFF-MD. They found the reaction between NH_2·and C atoms in coal is the primary path of N transfer. These research achievements fully demonstrate the powerful ability of molecular dynamics simulation technology in revealing microscopic mechanisms. However, MD simulation in the SS and coal co-gasification has not been systematically carried out. Specifically, the functioning mechanism of free radicals during the gasification process and their regulatory effects on product distribution remain unexplored.

In this study, the reaction mechanism of sludge and coal co-gasification was analyzed for the first time by using the ReaxFF – MD method. The key roles of OH and H radicals were revealed through analyzing the dynamic evolution of radicals. Additionally, we investigate the effect of different temperature and gasifier types on syngas product distribution. These findings not only fill the gaps of existing studies in the microscopic reaction paths during the co-gasification process, but also provide theoretical basis for the optimization and upgrading of SS and coal co-gasification technology. This holds significant importance for advancing the industrial deployment of low-carbon energy technologies.

2. Research methods

In this study, a combination of model construction, molecular dynamics simulation and data analysis was used to explore the mechanism. The following sections elaborate on the methods in detail.

2.1. Model construction

The primary components of SS are cellulose, lipids and proteins, accounting for approximately 80 % [31]. It is difficult to analysis the gasification process using conventional methods [32]. In this study, three different monomers (β-D-glucose, triglyceride, and leucine) were chosen to represent cellulose, lipids, and proteins, as shown in Fig. 1 a-c. These monomers contain functional groups (such as carbonyl and carboxyl groups) and are key sites for reactions to take place [33]. Therefore, it is crucial to study the interactions of these monomer and coal.

Bituminous coal is characterized by high carbon content and low moisture content. This making it allow for more efficient conversion into

Table 1
The mass fraction of components in each system.

System		β-D-glucose	Glyceryl triacetate	Leucine	Coal	Water	CO_2
S1	Number of molecules	10	20	28	0	819	0
	Mass fraction	7.33 %	17.75 %	14.93 %	0	60 %	0
S2	Number of molecules	0	0	0	2	456	0
	Mass fraction	0	0	0	40 %	60 %	0
S3	Number of molecules	6	11	16	2	921	0
	Mass fraction	3.91 %	8.68 %	7.59 %	19.81 %	60 %	0
S4	Number of molecules	6	11	16	2	0	377
	Mass fraction	3.91 %	8.68 %	7.58 %	19.81 %	0	60 %

(S1: Sludge Steam Gasification System, S2: Coal Steam Gasification System, S3: Sludge and coal steam co-gasification System, S4: Co-gasification system with CO_2).

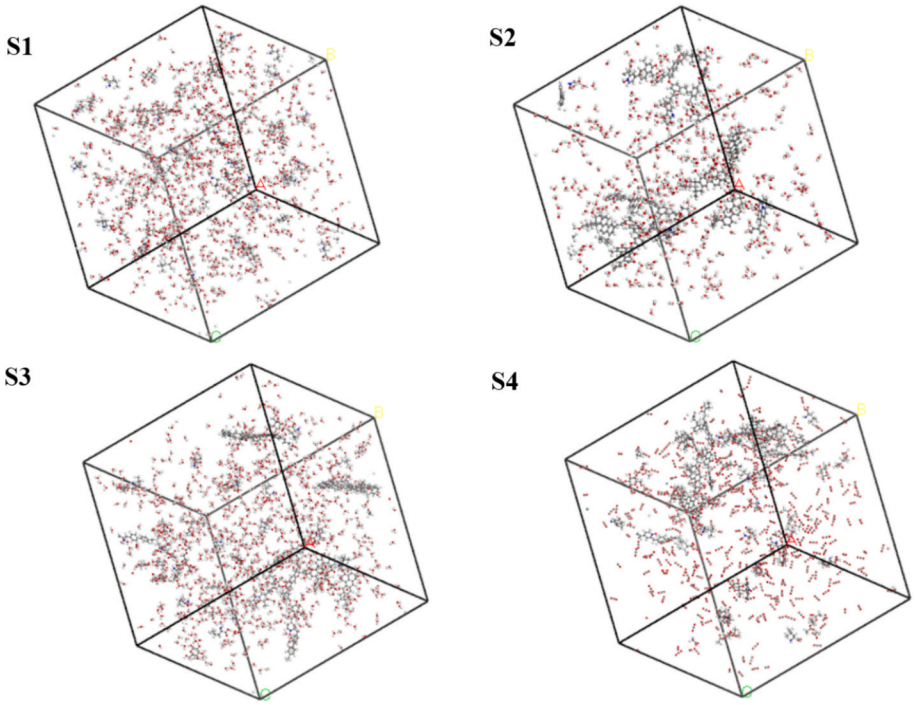

Fig. 2. Optimized model systems for gasification. (S1: Sludge Steam Gasification System, S2: Coal Steam Gasification System, S3: Sludge and coal steam co-gasification System, S4: Co-gasification system with CO_2).

synthesis gas. The bituminous coal model developed by Xu et al. [34] is employed in this study. Fig. 1(d) shows the molecular structure of bituminous coal with formula $C_{192}H_{167}O_{14}N_3$ and molecular weight of 2737.

Different systems were constructed by using the Amorphous Cell module in Materials Studio. Systems density were set to 0.1 g/cm^3 to prevent overlapping systems between atoms [35]. Table 1 presents the number and the mass fractions of molecules in each system, where the proportion of components in S1 is referenced from sludge sample from Djandja et al. [36]. The structure was then optimized using the Forcite module. The steepest descent and conjugate gradient methods were used to determine the lowest-energy conformations. Fig. 2 presents the four systems following optimization.

2.2. Simulation details

These systems were imported into the LAMMPS software to conduct MD simulations under periodic boundary conditions and an NVT conditions. Given the multi-element composition (C, H, O, N) of these systems, the employment of the C/H/O/N ReaxFF reactive force field file developed by Mitchell A. Wood et al. [37] is justified. This file was used to accurately describe atomic interactions in the reactions of thermal conversions. For example, Hong et al. [38] employed this field to conduct a simulation study on the synergistic effect mechanism of H_2 generation during the co-pyrolysis of coal and NH_3. During the simulation process, the Berendsen thermal bath method was employed to control the system temperature, with a time step set at 0.25 fs and a total simulation duration of 1325 ps. To ensure that the systems reached thermodynamic equilibrium, all systems underwent a relaxation time of 25 ps at a relaxation temperature of 300 K.

The time scales simulated by ReaxFF-MD are on the order of picoseconds, which is a smaller timescale than that of the actual chemical reactions. In accordance with the temperature-accelerated reaction kinetics theory (TTS) [39] and Arrhenius' law [40], elevating the temperature enhances reaction rates without modifying the reaction mechanisms. Meanwhile, prior investigations have demonstrated that thermal increases exert a negligible influence on reaction products and mechanistic pathways [41]. Consequently, the simulation temperature was raised to 2000 K-3500 K in this study. Multiple simulations were performed with randomized initial conditions (molecular positions and velocities) to minimize inherent uncertainties. Finally, the reaction process was observed using the visualization software VMD and the product files were analyzed using Python. Researchers may request the data by contacting the corresponding author.

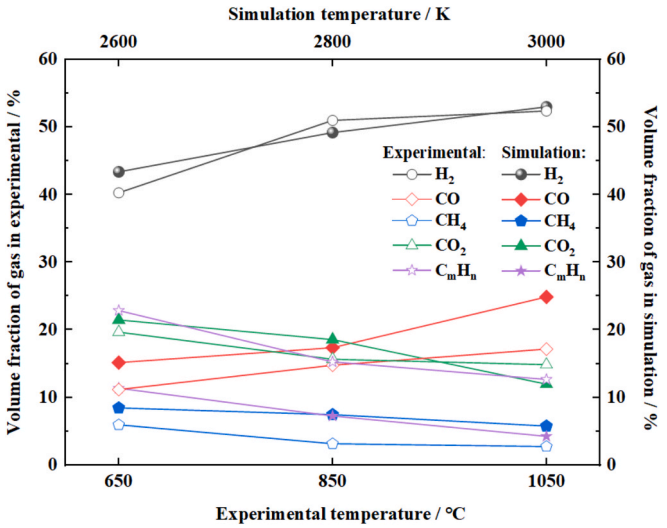

Fig. 3. Variation of volume fraction of different gas products with temperature.

2.3. Evaluation indicators

To evaluate the synergy of the co-gasification process, the following formula was used:

$$\Delta n = n_{i,experiment} - n_{i,theory} (i = 1, 2 \cdots)$$

where 'i' represents the various gases, '$n_{i,experiment}$' represents the actual amount of gas substance per kg in the SS and coal steam co-gasification system, and '$n_{i,theory}$' represents the theoretical amount of gas substance per kg in the same system. A positive value of Δn indicates a positive synergistic effect of the co-gasification reaction on the gas. The strength of the synergistic effect can be determined based on the magnitude of the value. All data provided corresponds to the dry ash-free basis.

3. Results and discussion

In this section, the models are verified, and the role of free radicals in the co-gasification process is clarified through the simulation data. These discussions and results are presented in the subsequent sections.

3.1. Model verification

To verify the accuracy and applicability of the SS model, the simulation results for S1 were compared with the gasification products obtained by Hu et al. [42] in their high-temperature steam gasification experiments on SS. Fig. 3 illustrates the changes in the volume fractions of the five main gas products (H_2, CO, CH_4, CO_2, C_nH_m), which account for approximately 90 % of the total gas products. The trends of the main gas products obtained from the MD simulation results are in good agreement with the experimental results, thereby fully verifying the reliability of the simulation model [43]. Moreover, the volume fractions of the main gases produced in the two results are approximately equal. This finding further validates the reliability of the sludge model employed in this study.

3.2. Analysis of synergies

This section outlines the isothermal transition behaviors of the S1, S2, and S3 systems at a temperature of 3000 K. Some gases (such as C_2H_6, C_2H_4, HCHO) were deemed negligible due to their low concentrations. The major gas products accounted for, including H_2, CO, CH_4, CO_2, NH_3, and C_2H_2, are constituted to make up over 80 % of the total gas products in the system. Fig. 4a presents these volume fractions of major gas products among systems S1, S2, and S3. It was observed that the process in S3 produced greater quantities of flammable gases (H_2 and CO).

Fig. 4b shows the actual and theoretical yields of the main gaseous products per kilogram of the SS and coal mixture in the co-gasification process. There is a positive synergistic effect on the production of H_2 (Δn = +5.57 mol/kg) and CO (Δn = +3.15 mol/kg), while its impact on CO_2 and NH_3 production is relatively minor during the co-gasification process. For CH_4, the actual values closely align with the theoretical values, suggesting that it does not enhance CH_4 production in co-gasification process. In contrast, the actual value for C_2H_2 is lower than the theoretical value, implying a negative synergistic effect on its production. This finding aligns with the experimental results reported by García et al. [44]. Additionally, the theoretical and actual values for water vapor consumption during co-gasification were calculated as $n_{i,theory} = 18.74 mol/kg$ and $n_{i,experiment} = 22.18 mol/kg$, respectively. These results indicate that the co-gasification process positively influences water vapor consumption, thereby promoting the production of H_2 and CO.

3.3. Main processes of sludge and coal gasification

This section investigates the consumption of steam molecules and major gas products in the system at a temperature of 3000 K. Fig. 5 illustrates the trends in the number of water molecules and main gas products generated over time. Initially, the number of H_2O molecules in the different systems remains stable as the simulation progresses. Subsequently, the amount of H_2O in the S1, S2 and S3 systems started to decrease at 108.55 ps, 95.18 ps and 70.78 ps, respectively. Meanwhile,

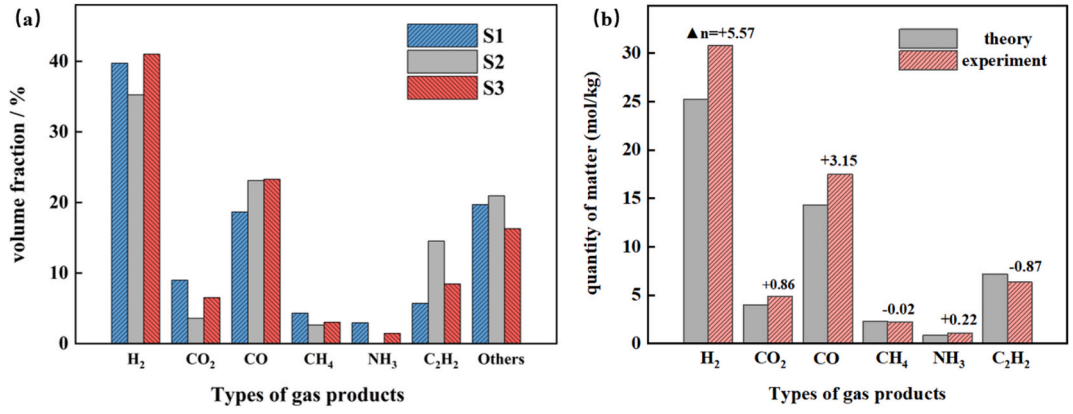

Fig. 4. (a)Volume fraction of each gas product in different systems. (b) Comparison of the actual and theoretical values of the quantities of substances in the main gas products.

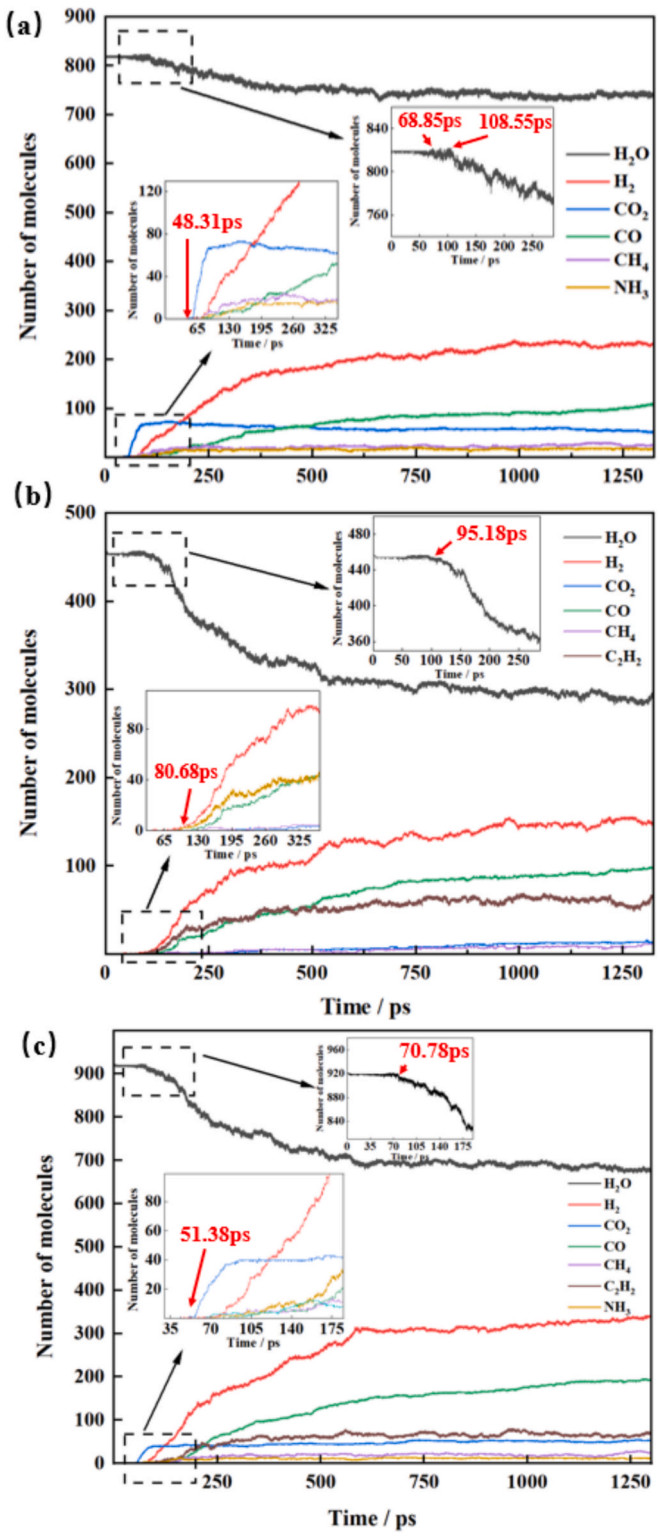

Fig. 5. The number of water molecules and major gas products varies with simulation time in different systems. (a)S1: Sludge Steam Gasification System, (b)S2: Coal Steam Gasification System, (c)S3: Sludge and coal steam co-gasification System.

the first gas production events in the three systems occurred at 48.31 ps (CO_2) for S1, 80.68 ps (H_2) for S2, and 51.38 ps (CO_2) for S3, respectively. Through comparison, it was found that the generation time of the main gas products precedes the decrease in the number of H2O molecules. Therefore, the reaction process can be divided into two stages: the pyrolysis stage and the gasification stage. In the pyrolysis stage, the macromolecules of SS and coal components undergo cracking. Due to the aliphatic side-chain components are particularly prone to cracking [45], this results in the formation of a small amount of gaseous hydrocarbons. During the gasification stage, a substantial number of H_2O molecules participate in the reaction. As the reaction proceeds, substantial amounts of gases are produced.

In addition, the number of H_2O molecules began to fluctuate and slightly increase at 68.85 ps in S1. This could be because, the cracking of sludge generates a small amount of H_2O molecules during the pyrolysis stage.

3.4. Analysis of sludge and coal co-gasification mechanism

To clearly understand the co-gasification mechanism of SS and coal, further analysis was conducted using VMD software and simulation data. Fig. 6 illustrates the sequential reactions of glyceryl triacetate molecule ($C_9H_{14}O_6$), leucine molecule ($C_6H_{13}O_2N$), monomeric β-D-glucose ($C_6H_{12}O_6$), and bituminous coal molecule ($C_{192}H_{167}O_{14}N_3$) during this process. Due to the lower bond energy of its C-O-C bonds compared to the C–C and C–H bonds [46], $C_9H_{14}O_6$ undergoes cleavage at 47.18 ps. This process generates the $C_2H_3O_2$ group and allyl radical (C_3H_5), as depicted in Fig. 6a. At 56.25 ps, $C_6H_{13}O_2N$ experiences successive cleavage of C–C bonds. Fig. 6b shows that it fragments into smaller molecules while generating CO_2 in this process. At 62.28 ps, the ether bond in $C_6H_{12}O_6$ breaks to generate a $C_5H_{10}O_4$ group and a CH_2O_2 group, as shown in Fig. 6c. Additionally, a small amount of H radicals is generated during the pyrolysis process, which facilitates subsequent reactions. These observations align with the findings of Hao et al. [47].

Fig. 6d shows the typical reaction process in coal molecules break down and decompose into smaller molecular groups during the pyrolysis stage. The hydroxyl groups connected to nitrogen atoms in coal molecules are highly unstable at high temperatures. Consequently, the detachment of OH group results in the formation of a $C_{192}H_{166}O_{13}N_3$ group from coal molecules. The bond energy of ether bonds linked to aliphatic groups is lower than that of ether bonds in aromatic groups [45]. Thus, the ether bonds in the $C_{178}H_{154}O_{12}N_2$ group attached to the aliphatic component break first. This leads to the formation of the $C_{147}H_{128}O_{11}N$ group and the small molecular fragment $C_{31}H_{26}ON$. Within the $C_{147}H_{128}O_{11}N$ group, the C-O and C–C bonds in the six-membered ring containing oxygen also break, resulting in the $C_{63}H_{60}O_4$ group and the nitrogen-containing $C_{84}H_{68}O_7N$ group. Subsequently, the ether bond linked to the aliphatic group in the $C_{63}H_{60}O_4$ group also broke, resulting in the formation of the molecular fragments ($C_{30}H_{27}O_2$ and $C_{33}H_{33}O_2$). Finally, the C–C bond was cleaved and the ether bond attached to the aromatic group in the $C_{84}H_{68}O_7N$ group was broken. This led to the generation of the five-membered ring containing oxygen (C_7H_9O), along with the small molecular fragments $C_{23}H_{20}O_2$ and the $C_{54}H_{39}O_4N$ group.

During the pyrolysis stage, a large number of molecular fragments are produced. Among them, aromatic rings exhibit higher stability compared to chain hydrocarbons [29]. Based on this, it is necessary to deeply analyze the role of free radicals in the transition mechanism during the co-gasification process. Fig. 7 shows the changes in the mass fraction of free radicals in different systems. The generation of OH and H radicals increased rapidly within the range of 50 ps to 200 ps, which indicates that H_2O are involved in the reaction of gasification stage. As the gasification reaction progresses, the number of OH radicals decrease significantly before 300 ps in Fig. 7a. This suggests that OH radicals play a role at early stage of gasification. While for the H radicals in Fig. 7b, a sharp decrease occurs after 300 ps, indicating that H radicals mainly react at the later gasification stage. Additionally, it was found that the number of H radicals in S2 is higher than that in S1 and S3. This indicates that the addition of coal in co-gasification is conducive to the consumption of H radicals from SS.

As illustrated in Fig. 8, the interactions between OH radicals and

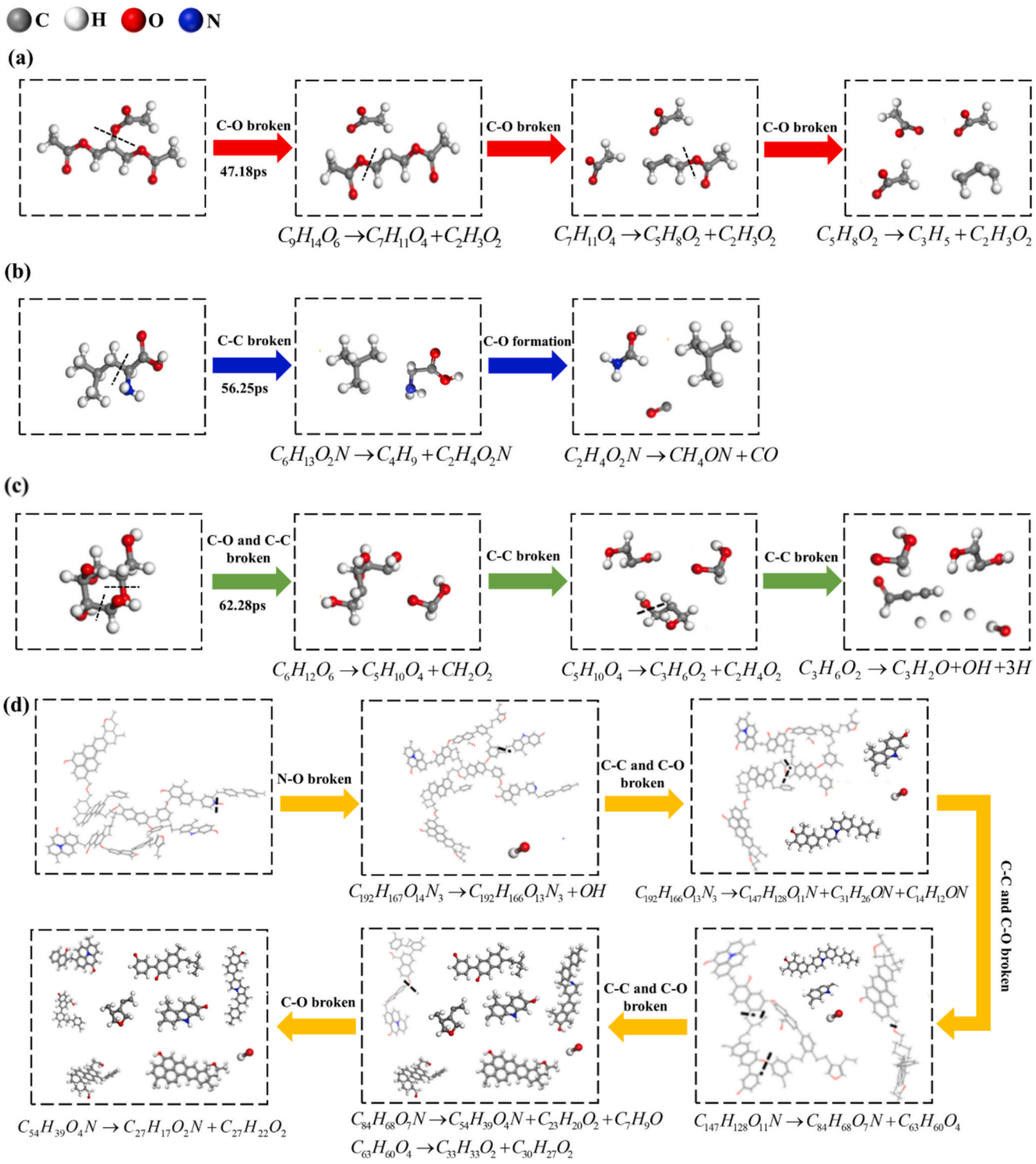

Fig. 6. Pyrolysis of molecules in the pyrolysis phase of a co-gasification reaction. (a) glyceryl triacetate molecule ($C_9H_{14}O_6$), (b) leucine molecule ($C_6H_{13}O_2N$), (c) monomeric β-D-glucose ($C_6H_{12}O_6$), (d) bituminous coal molecule ($C_{192}H_{167}O_{14}N_3$).

molecular fragments formed during pyrolysis are categorized into three pathways. The first pathway (red) shows that OH radicals can attack cyclic structures, thereby forming chain-like structures or small molecular groups [46]. For example, OH radicals substitute hydrogen atoms on the benzene ring of $C_{14}H_{12}ON$, triggering ring cleavage to form $C_{11}H_9O_2N$ and a propargyl group (C_3H_3). The second pathway (blue) involves OH radicals reacting with oxygenated chain groups produced during pyrolysis, leading to the formation of reactive intermediates. For instance, OH radical abstract hydrogen atoms from the methyl group of $C_6H_{14}O$ yielding the reactive intermediate $C_6H_{14}O_2$ and a H free radical. The third pathway (green) shows that OH radicals react with hydrocarbon molecules (C_5–C_{15}) in the pyrolysis stage, also generating reactive groups. Collectively, these results indicate that abundant OH radicals predominantly attack molecular fragments, converting them into small-molecule highly reactive groups.

In the later gasification stage, the H radicals more readily react with the already generated small-molecule highly reactive groups and are further cleaved to produce gaseous products. These highly reactive

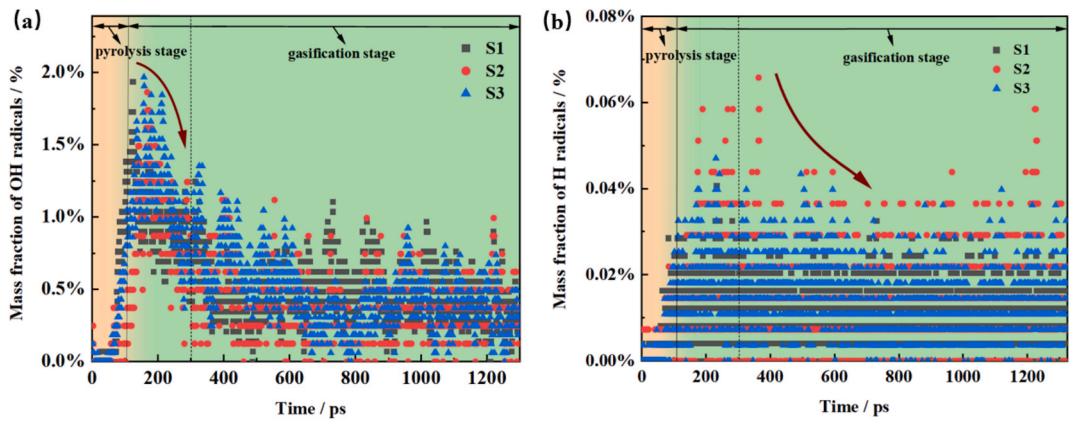

Fig. 7. Comparison of the mass fraction of OH and H during the reaction process of different systems. (a) OH radicals; (b) H radicals.

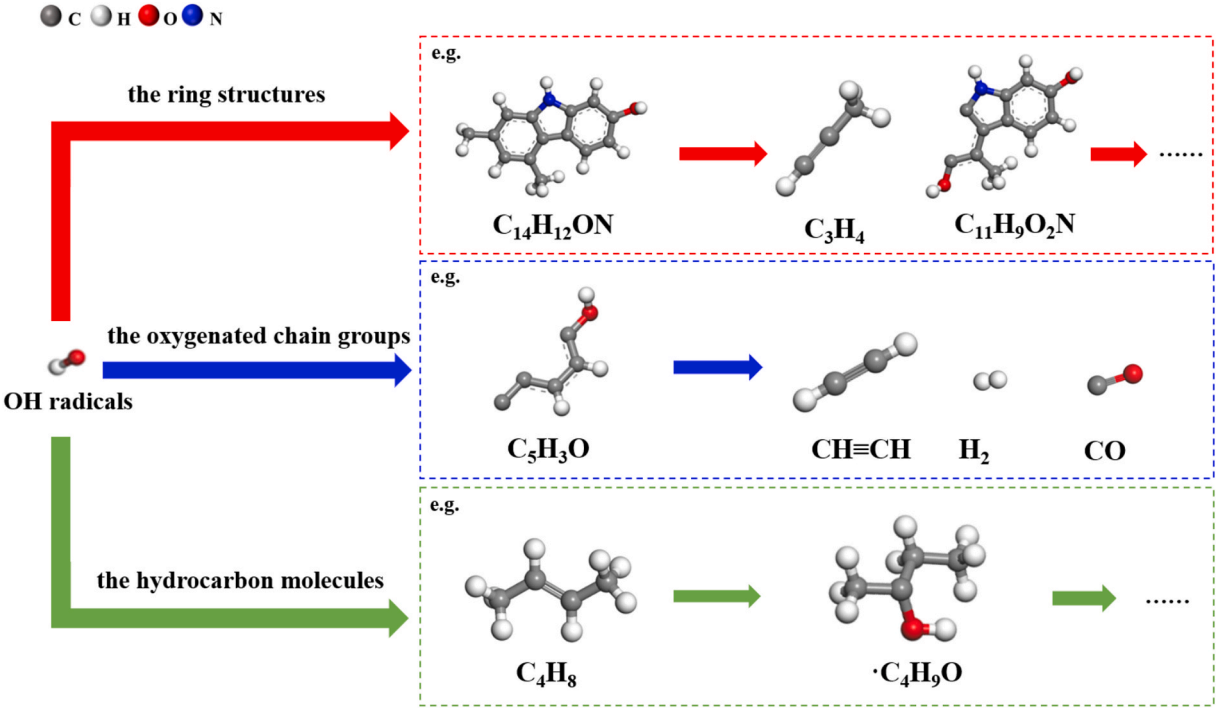

Fig. 8. Typical examples of OH radicals interacting with various small molecule fragments produced by pyrolysis.

groups can be classified into oxygen-containing groups and non-oxygen-containing groups, as shown in Fig. 9. For oxygen-containing groups, the reactions can be subdivided into three categories: reactions involving carbonyl groups (C═O), carboxyl groups (COOH), and ether bonds (−O–). These groups are ultimately converted into CO or CO_2 under the action of H radicals. This is highly consistent with the findings of Qiu et al. [40]. For non-oxygenated groups, H radicals induce cleavage of C–C bonds, thereby generating small-molecule hydrocarbon gases. In addition, H radicals can react with the NH_2 radicals to generate NH_3 ultimately.

Overall, the generation of OH and H radicals facilitates the reaction between SS and coal during the co-gasification process. These free radicals promote the conversion of complex organic structures into small molecules, thereby minimizing the formation of secondary coke and tar.

3.5. *Influencing factors on the synergistic effect*

The efficiency of product formation and component distribution are influenced by temperature and gasifier type. The subsequent sections explore these factors.

3.5.1. *Influence of temperature*

This section explores the impact of different temperature on the co-gasification process. Fig. 10 illustrates the trend of gas product molecule quantities at different temperatures in S3. The activation energy barriers for the aromatic rings typically range from 364.66 to 477.6 kJ/mol [48]. Therefore, when the simulated equilibrium temperature is too low, the aromatic structures cannot undergo ring-opening reactions with OH radicals. This indirectly results in a significant reduction in the number of H_2 and CO molecules. As shown in Fig. 10 c-d, the yield of CO_2 is lower than that at 2500 K and 3000 K. It indicates the existence of a saturation point in the reaction. This saturation point also occurs in the generation of CH_4. This phenomenon can be attributed to the fact that at higher temperatures, the dry reforming of methane (DRM) reaction is promoted, converting CH_4 and CO_2 into syngas [34].

For further analysis, we counted the volume fractions of the four gas products. Fig. 11 shows that the increase in temperature has increased

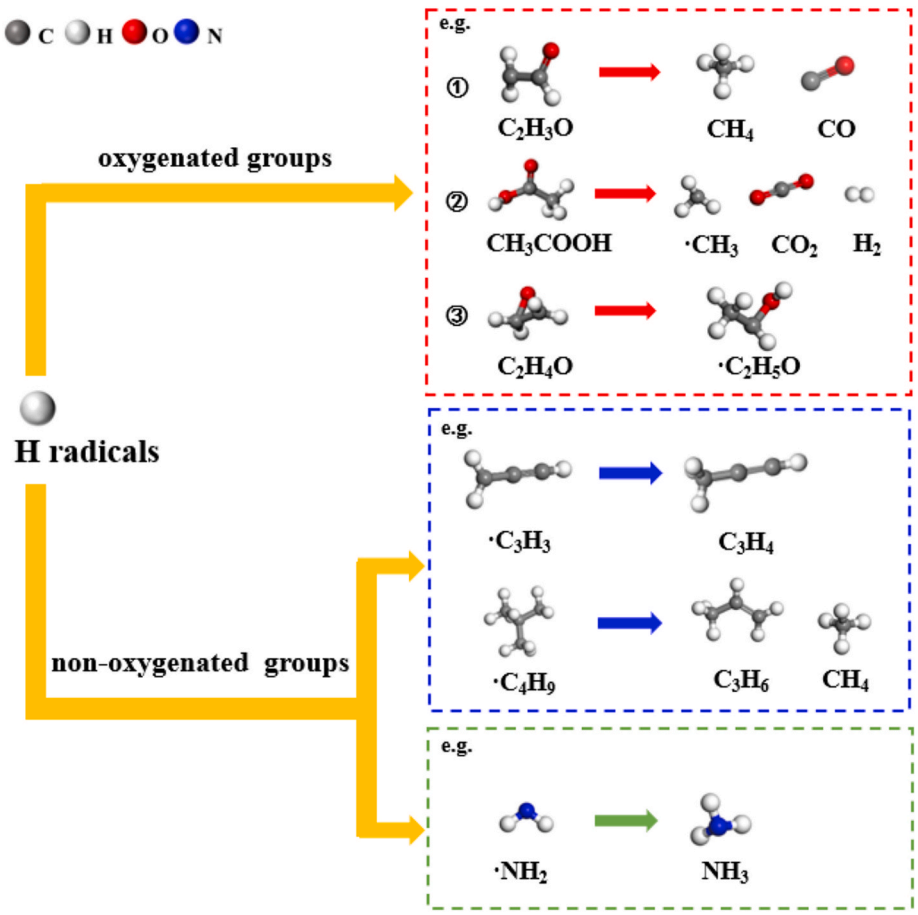

Fig. 9. Typical examples of H radicals interacting with various small molecule fragments produced by pyrolysis.

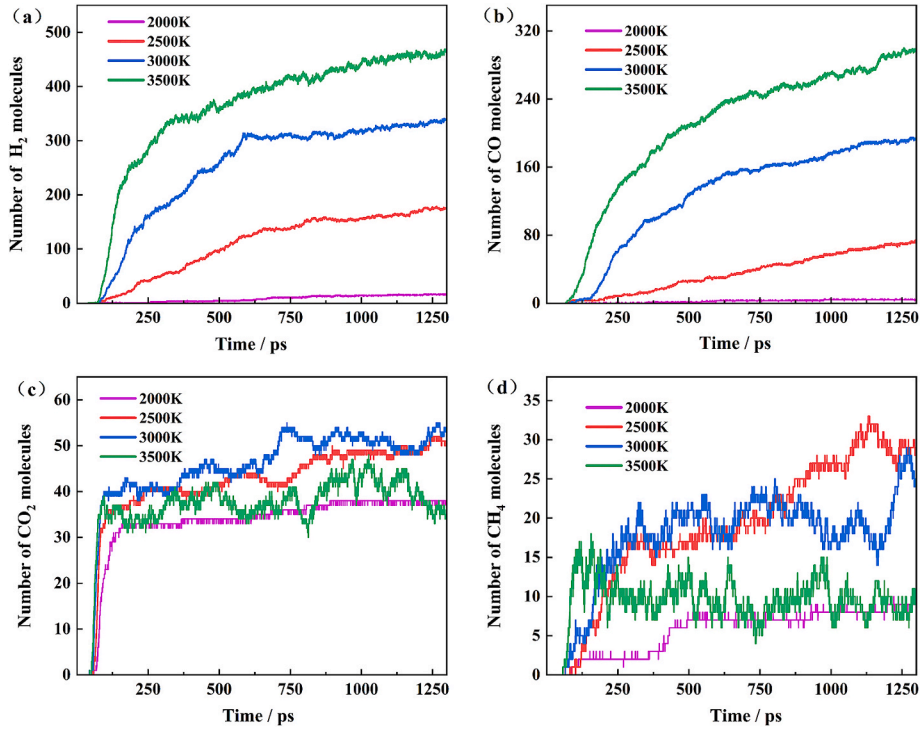

Fig. 10. Variation of the number of gas molecules with simulation time at different temperatures (a) H_2; (b) CO; (c) CO_2; (d) CH_4.

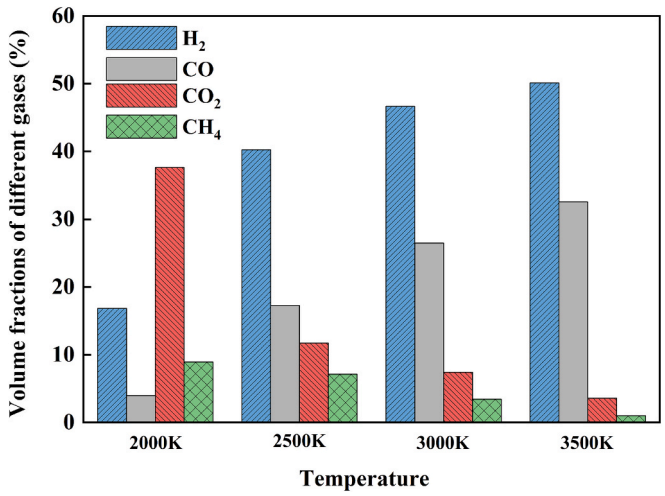

Fig. 11. Volume fractions of gas products at different simulated temperatures.

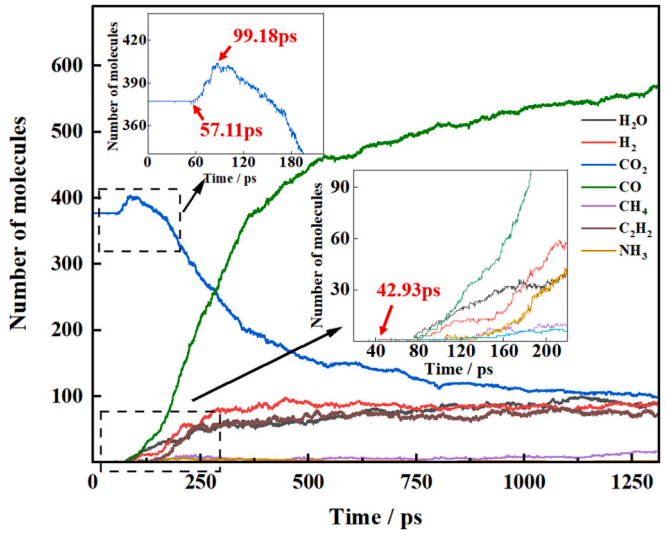

Fig. 12. Changes in the number of different gas products over simulation time in S4.

the yields of H_2 and CO by 33.3 % and 28.6 % respectively. Conversely, the volume fractions of CO_2 and CH_4 continuously decline by 34.1 % and 7.9 % respectively when the equilibrium temperature rises. Therefore, the right temperature needs to be chosen to regulate the distribution of the gasification products.

3.5.2. Influence of gasifying agent

This section delves into the influence of different gasifying agents on the co-gasification process. Fig. 12 shows the variations in the number of CO_2 molecules and key gas products over time at a temperature of 3000 K in S4. During the pyrolysis stage, the amount of CO_2 remained nearly constant, consistent with the trend of water molecule counts in S3. This suggests that gasifying agents do not participate in the reaction, while macromolecules undergo cleavage within the system during the initial reaction stage. Starting from 57.11 ps, the number of CO_2 molecules increased rapidly. The peak of the curve occurs at 99.18 ps due to the small amount of CO_2 generated from the cleavage of the sludge components. Upon entering the gasification stage, gaseous products are gradually produced in the system. CO began to form after the production of H_2O molecules, and its quantity initially increased rapidly and then slowed down. Subsequently, H_2, NH_3, C_2H_2, and CH_4 were produced in sequence. The generation trends of H_2 and C_2H_2 were very similar to

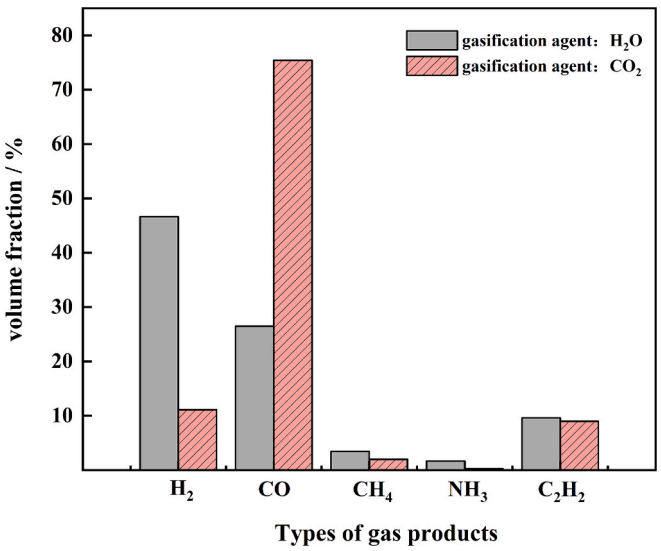

Fig. 13. Comparison of volume fractions of gas products with different gasifying agents.

that of H_2O, while the generation changes of CH_4 and NH_3 exhibited a similar pattern. This variation trend are consistent with the experimental results of Khalil et al. [49].

Once the S4 system attained a steady state, statistical analysis of the gas products was performed. The results indicate that five major gas products constitute 97.74 % of the total gas volume (excluding H_2O), as depicted in Fig. 13. When CO_2 is used as the gasifying agent, it significantly enhances both the quantity and percentage of CO molecules in the gas products, with a growth rate of 48.9 %. In sharp contrast, the number of H_2 molecules and their percentage content decrease significantly, with a decline rate of 35.5 %. The ratio of H_2 to CO also drops from 1.76 to 0.15, consistent with the experimental findings of Han et al. [50].

To explore the mechanism further, the mass fraction of OH and H radicals under the influence of different gasifying agents was counted. Fig. 14 shows that the content of OH radicals in S4 is significantly lower than that in S3. This induces the incapability of ring structures to undergo cleavage, thereby triggering accumulation and coke formation. The high yield of CO is associated with the reaction of CO_2 with coke during the initial gasification stage [51]. Meanwhile, the decrease of small reactive group results in an accumulation of free H radicals in the system. As the gasification reaction progresses, these H radicals react with small highly reactive groups to produce gaseous products. Therefore, while the type of gasifying agent generally does not alter the main gas compositions of SS and coal co-gasification, it does influence the H_2/CO ratio, with minimal impact on other gas products.

4. Conclusions

In this study, β-D-glucose, glyceryl triacetate, and leucine were selected as molecular models for cellulose, lipids, and proteins in sewage sludge respectively. A sewage sludge steam gasification system was constructed, and the reliability of the model was verified through experiments data. Statistical analysis of the ReaxFF-MD simulation results confirmed that there is a significant synergistic effect during the co-gasification process. The yields of H_2 and CO increased significantly by 2.1 % and 1.75 % respectively, while the yields of gases such as CO_2, NH_3, and CH_4 were basically unaffected, and the formation of C_2H_2 was inhibited.

Through visual analysis using VMD software, it was found that the co-gasification reaction is primarily driven by OH and H radicals. During the pyrolysis stage, glyceryl triacetate, leucine, β-D-glucose, and

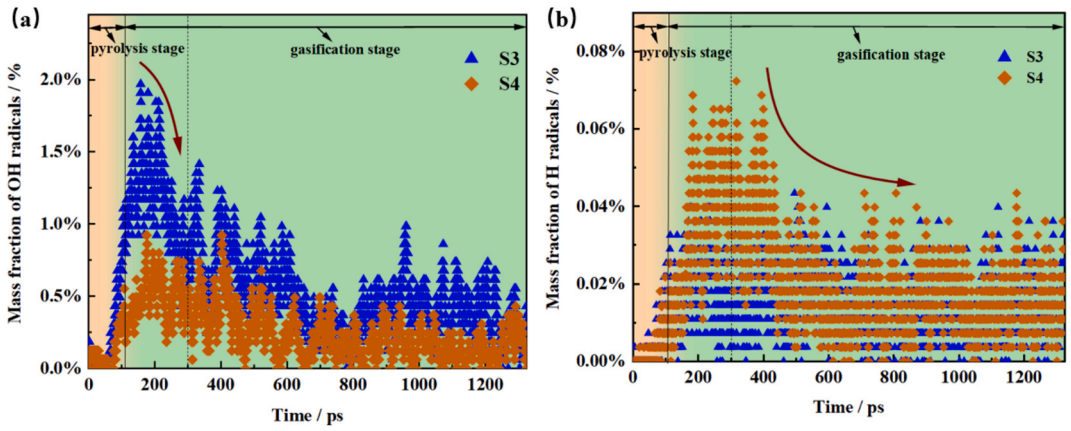

Fig. 14. Comparison of the mass fraction of OH and H in the reaction of different gasifying agents. (a) OH radicals; (b) H radicals.

bituminous coal were sequentially decomposed into molecular fragments, releasing a number of OH and H radicals. In the gasification stage, OH radicals first react with cyclic structures, oxygen-containing chain structures, and hydrocarbon gases to form highly reactive small molecular groups. Subsequently, H radicals are more likely to react with these highly reactive groups. Specifically, H radicals can react with both oxygen-containing groups such as carbonyl, carboxyl, and ether bonds and oxygen-free reactive groups to produce gaseous products. In addition, temperature and the type of gasifying agent have an important impact on the product distribution. Increasing the temperature accelerates the fragmentation of molecules and promotes the conversion of CH_4 and CO_2 into syngas. When CO_2 is used as the gasifying agent, the generation amount of OH radicals decrease. This promotes the full reaction between CO_2 and coke and significantly increases the volume fraction of CO.

In the future, researchers can build a multicomponent modeling system for actual sludge to evaluate the impact on the carbon conversion pathway. Moreover, a directed catalytic system based on free radical modulation could be developed. This study offers a feasible pathway for industrial decarbonization and a theoretical foundation for optimizing the co-gasification of sludge and coal.

CRediT authorship contribution statement

Jian Gao: Writing – review & editing, Writing – original draft, Supervision. **Weiwei Xuan:** Writing – review & editing, Supervision. **Erzhou Zhang:** Writing – review & editing, Supervision. **Yaqiong Wang:** Writing – review & editing, Supervision. **Jiansheng Zhang:** Writing – review & editing, Supervision. **Qi Wang:** Writing – review & editing, Supervision.

Declaration of competing interest

The authors declare that they have no known competing financial interests or personal relationships that could have appeared to influence the work reported in this paper.

Acknowledgements

This work is supported by the National Natural Science Foundation of China (52276098) and Youth Program of Shanxi Research Institute of Huairou Laboratory (2023SY3003).

Data availability

Data will be made available on request.

References

[1] Shindell D, Smith CJ. Climate and air-quality benefits of a realistic phase-out of fossil fuels. Nature 2019;573:408–11.
[2] Panagiotis F, van Soest Heleen L, Roberto S, Luke R, C. KA, Nick M, et al. Energy system transitions and low-carbon pathways in Australia, Brazil, Canada, China, EU-28, India, Indonesia, Japan, Republic of Korea, Russia and the United States. Energy (Oxf) 2021;216. 119385.
[3] Wei Y, Chen K, Kang J, Chen W, Wang X, Zhang X. Policy and management of carbon peaking and carbon neutrality: a literature review. Engineering (Beijing) 2022;14:52–63.
[4] Gong S, Ge Z, Zhang X, Zhou X, Huang S, Lu C, et al. Microstructure characteristics of bituminous coal under the synergistic effect of VES, acids and oxidants: Implications for CO2 injection capacity. Energy (Oxf) 2025;317:134618.
[5] Tomaiuolo G, Carnieletto L, Pecchini M, Benato A, Stoppato A, De Carli M. Optimization and assessment method to approach industrial site decarbonization: A case study of a light industry. Energy Convers Manag 2025;326:119460.
[6] Thiel GP, Stark AK. To decarbonize industry, we must decarbonize heat. Joule 2021;5:531–50.
[7] Chen W, Wei C, Sun L, Dong H, Hijioka Y, Nakajima K, et al. Carbon-neutral heat supply strategies for industrial decarbonization: A critical and systematic literature review. Cleaner Respon. Consumpt. 2024;15:100244.
[8] Wang C, Qiao H, Yan R, Liu X, Deng L, Che D. Thermodynamic and economic evaluation of a novel waste-to-energy system combining biogas power generation and sewage sludge pyrolysis. Energy Convers Manag 2025;327:119531.
[9] Ni Z, Zhang Y, Liu X, Shi H, Yao Y, Tian J, et al. Effect of furnace temperature and oxygen concentration on combustion and CO/NO emission characteristics of sewage sludge. Renew Energy 2024;234:121225.
[10] Hamze A, Zakaria BS, Zaghloul MS, Ganatsios A, Chrysochoou D, Dhar BR, et al. Novel bioaugmentation process to enhance anaerobic digestion of municipal sewage sludge. Renew Energy 2024;236:121370.
[11] Ogugua PC, Su H, Wang E. Synergistic blending of biomass, sewage sludge, and coal for enhanced bioenergy production: Exploring residue combinations and optimizing thermal conversion parameters. J Environ Manage 2024;352:120035.
[12] Hui L, Sujie S, Xueying L, Dapeng L, Yong H. Preparation of cationic aggregates derived from sewage sludge for efficient capture of organic matter. Chemosphere 2023;333:138909.
[13] Deng J, Tang Y, Tang J, Liu H, Chen W, Sun Z, et al. From sewage sludge to Hydrogen: Life cycle Techno-Environment-Economic assessment of combined system with supercritical water Gasification, organic Rankine cycle and carbon capture and storage. Energy Convers Manag 2025;323:119221.
[14] Dai Y, Liu G, Liang H, Fang H, Chen J, Wang F, et al. Co-gasification characteristics of Ca-rich sludge and Fe-rich sludge under CO2 atmosphere, and potential utilization of gasification residues as renewable catalyst in biomass pyrolysis. Renew Energy 2024;224:120118.
[15] Zhang X, Shi S, Men X, Hu D, Yang Q, Zhang L. Elevating clean energy through sludge: A comprehensive study of hydrothermal carbonization and co-gasification technologies. J Environ Manage 2024;369:122388.
[16] Hantoko D, Kanchanatip E, Yan M, Lin J, Weng Z. Co-gasification of sewage sludge and lignite coal in supercritical water for H 2 production: a thermodynamic modelling approach. Energy Procedia 2018;152:1284–9.
[17] He Y, Li X, Meng L, Zhang W, Wang Y, Wang L, et al. Experimental investigation on high-temperature co-gasification and melting behavior of petrochemical sludge and bituminous coal in CO2 atmosphere. Energy (Oxf) 2024;303:131931.
[18] Mosqueda A, Wei J, Medrano K, Gonzales H, Ding L, Yu G, et al. Co-gasification reactivity and synergy of banana residue hydrochar and anthracite coal blends. Appl Energy 2019;250:92–7.
[19] Wang C, Feng H, Jin H. Regulation mechanism of phenol on intermediates during supercritical water gasification of coal. Int J Hydrogen Energy 2024;88:385–94.
[20] Ma M, Zhang S, Chen Y, Chen B, Guo L. Optimization of hydrogen-rich syngas from coal and sewage sludge co-gasification in supercritical water. Chem Eng J 2024; 497:154792.

[21] Wei F, Mo Z, Lijun J, Jin B, Lingxue K, Huaizhu L, et al. Co-pyrolysis behaviors of coal and polyethylene by combining in-situ Py-TOF-MS and reactive molecular dynamics. Fuel (Lond) 2023;331.
[22] Kai W, Hai Z, Xin W, Weidong F. Study on pyrolysis mechanism of coal in hydrogen-rich atmosphere based on reactive molecular dynamics simulation. Int J Hydrogen Energy 2024;49:861–72.
[23] Wenjun Z, Weixing Z, Huayu Q, Dun L, Yu Z, Sajjad AM, et al. Tuning the reactivity of Ni/MoS2 membrane for efficient methane pyrolysis and hydrogen production: A multi-scale study. Energy Convers Manag 2023;293.
[24] Svobodova-Sedlackova A, Barreneche C, Alonso G, Fernandez AI, Gamallo P. Effect of nanoparticles in molten salts – MD simulations and experimental study. Renew Energy 2020;152:208–16.
[25] Xia S, Shen C, Lin J, Tu M, Tan CP, Cheong LZ. Enhanced methanol tolerance of ZIF-8-immobilized Aspergillus oryzae lipase for biodiesel production from used cooking oil. Renew Energy 2025;239:122122.
[26] Huang Z, Liu H, Hao J, Zhou W, Wu Z, Wei J. Mechanistic exploration of tar-rich coal pyrolysis through ReaxFF MD simulation coupled with experimental validation. J Energy Inst 2025;118:101940.
[27] Wei Y, Wu Y, Du Z, Zhang X, Xu J, Xu K, et al. Interaction mechanisms of coal macerals during pyrolysis: Insights from TG and Py-GC/MS experiments combined with ReaxFF MD simulations. Chem Eng J 2025;504:158768.
[28] Weiwei X, Jian G, Zhen M, Chunyan C, Shiying Y, Qi W. Synergistic mechanism and radicals interaction of the co-pyrolysis of lignite and PE based on ReaxFF-MD and DFT. Energy (Oxf) 2024;289:129978.
[29] Wang Le, Li A, Peng Z, Yi L, Chen B, Jin H, et al. Investigation on the detailed mechanisms of cationic ion exchange resin gasification in supercritical water by ReaxFF reactive molecular dynamics simulation. Biomass Bioenergy 2025;193:107586.
[30] Mengwei Y, Xin Y, Dunxi Y, Xi J. Molecular dynamics investigation of the effect of ammonia on coal pyrolysis and the nitrogen transformation. Energy Convers Manag 2023;285.
[31] Gao J, Weng W, Yan Y, Wang Y, Wang Q. Comparison of protein extraction methods from excess activated sludge. Chemosphere 2020;249:126107.
[32] Yang N, Ji H, Yang S. Influence of monosaccharides and lipids on protein structure and solubility-Reaction simulation of sludge thermal hydrolysis system. Bioresour Technol 2024;418:131940.
[33] Yang N, Yang S. Neglected sludge solid phase in sludge pretreatment process: Physicochemical characterization and mechanism study of its role in anaerobic degradation. Sci Total Environ 2024;944:173769.
[34] Tong X, Chunbo W, Dikun H, Song L, Shuang Y. The synergistic effect during co-combustion of municipal sludge and coal: Experimental and ReaxFF molecular dynamic study. Energy (Oxf) 2023;262.
[35] Yunhui P, Xiaoli Z, Ning L, Zhenbo W. Investigation on reaction mechanism for CO2 gasification of softwood lignin by ReaxFF MD method. Energy (Oxf) 2023;267.
[36] Sangué DO, Shimin K, Zizhi H, Junqiao L, Jiaqi F, Zaiming T, et al. Machine learning prediction of fuel properties of hydrochar from co-hydrothermal carbonization of sewage sludge and lignocellulosic biomass. Energy (Oxf) 2023;271.
[37] Wm A, van Duin ACT, Alejandro S. Coupled thermal and electromagnetic induced decomposition in the molecular explosive αHMX; a reactive molecular dynamics study. Chem A Eur J 2014;118:885–95.
[38] Hong D, Guo Y, Wang C, Xu T, Ma S. The synergistic effect mechanism of H2 generation during coal/ammonia co-pyrolysis. Proc Combust Inst 2024;40:105678.
[39] So Rensen MR, Voter AF. Temperature-accelerated dynamics for simulation of infrequent events. J Chem Phys 2000;112:9599–606.
[40] Qiu Y, Zhong W, Shao Y, Yu A. Reactive force field molecular dynamics (ReaxFF MD) simulation of coal oxy-fuel combustion. Powder Technol 2020;361:337–48.
[41] Jingwei C, Chenxi W, Wenxue S, Yu B, Xiaomin W. Study on the mechanisms of hydrogen production from alkali lignin gasification in supercritical water by ReaxFF molecular dynamics simulation. Energy (Oxf) 2023;278.
[42] Hu Y, Chen J, Li G, Lu Y. An expeirmental investigation into mechanism of high temperature steam gasification of wastewater sewage sludge. Therm Sci 2017;22:248.
[43] Jingwei C, Qiteng W, Hongda W, Tian M, Jiaqiang E, Erwei L, et al. Molecular dynamic study on mechanisms of polyvinylidene fluoride decomposition by using supercritical water. Chem Eng J 2022;431.
[44] García G, Arauzo J, Gonzalo A, Sánchez JL, Ábrego J. Influence of feedstock composition in fluidised bed co-gasification of mixtures of lignite, bituminous coal and sewage sludge. Chem Eng J 2013;222:345–52.
[45] Huang J, He C. Pyrolysis mechanism of α-O-4 linkage lignin dimer: A theoretical study. J Anal Appl Pyrolysis 2015;113:655–64.
[46] Jingwei C, Yu B, Tian M, Qiteng W, Chenxi WEJ. Detailed mechanisms of amoxicillin decomposition in supercritical water by ReaxFF reactive molecular dynamics simulation. Chem Eng J 2023;451.
[47] Qi HW, Jun LX. Molecular dynamics investigation on the co-gasification of various components of sewage sludge in supercritical water. Fuel (Lond) 2023;334.
[48] Aljaž G, Joong KS, M KR, Mojca B, Nevan K, Andrej', et al. EpCAM homo-oligomerization is not the basis for its role in cell-cell adhesion. Sci Rep 2018;8:13269.
[49] Khalil R, Varhegyi G, Jaeschke S, Gronli MG, Hustad J. Co2 gasification of biomass chars: a kinetic study. Energy Fuels 2009;23:94–100.
[50] Long H, Zhonghui W, Pingjiang W, Guoqiang X, Lianming L, Jianhao Z, et al. Fluidized bed chemical looping gasification of sewage sludge with bituminous coal to produce H2 rich syngas: An examination on fuel synergy and reaction conditions. J Energy Inst 2023;111.
[51] Zhao B, Jin J, Li S, Liu D, Zhang R, Yang H. Co-pyrolysis characteristics of sludge mixed with Zhundong coal and sulphur contaminant release regularity. J Therm Anal Calorim 2019;138:1623–32.